JBC RESEARCH ARTICLE

Identification of an N6-methyladenosine-mediated positive feedback loop that promotes Epstein–Barr virus infection

Received for publication, December 17, 2020, and in revised form, March 10, 2021 Published, Papers in Press, March 16, 2021,
https://doi.org/10.1016/j.jbc.2021.100547

Dan-Ling Dai[1,‡], Xingyang Li[2,‡], Lin Wang[1,3,‡], Chu Xie[1], Yanan Jin[1,4], Mu-Sheng Zeng[1], Zhixiang Zuo[1,*], and Tian-Liang Xia[1,*]

From the [1]State Key Laboratory of Oncology in South China, Collaborative Innovation Center for Cancer Medicine, Guangdong Key Laboratory of Nasopharyngeal Carcinoma Diagnosis and Therapy, Sun Yat-sen University Cancer Center, Guangzhou, P. R. China; [2]Department of Temporomandibular Joint Surgery, Affiliated Stomatology Hospital of Guangzhou Medical University, Guangzhou Key Laboratory of Basic and Applied Research of Oral Regenerative Medicine, Guangzhou, P. R. China; and [3]Department of Nasopharyngeal Carcinoma and [4]Department of VIP Region, Sun Yat-sen University Cancer Center, Guangzhou, P. R. China

Edited by Ronald Wek

N6-methyladenosine (m^6A) is among the most abundant mRNA modifications, particularly in eukaryotes, and is found in mammals, plants, and even some viruses. Although essential for the regulation of many biological processes, the exact role of m^6A modification in virus–host interaction remains largely unknown. Here, using m^6A -immunoprecipitation and sequencing, we find that Epstein–Barr virus (EBV) infection decreases the m^6A modification of transcriptional factor KLF4 mRNA and subsequently increases its protein level. Mechanistically, EBV immediate-early protein BZLF1 interacts with the promoter of m^6A methyltransferase METTL3, inhibiting its expression. Subsequently, the decrease of METTL3 reduces the level of KLF4 mRNA m^6A modification, preventing its decay by the m^6A reader protein YTHDF2. As a result, KLF4 protein level is upregulated and, in turn, promotes EBV infection of nasopharyngeal epithelial cells. Thus, our results suggest the existence of a positive feedback loop formed between EBV and host molecules *via* cellular mRNA m^6A levels, and this feedback loop acts to facilitate viral infection. This mechanism contains multiple potential targets for controlling viral infectious diseases.

Epstein–Barr virus (EBV), a large double-stranded DNA virus belonging to the γ-herpesvirus subfamily, causes latent infection of more than 95% of the adult population worldwide (1, 2). As a widespread virus causing infectious mononucleosis during primary infection, EBV is also closely implicated in several malignancies in latent infection, including B-cell lymphomas, nasopharyngeal carcinoma (NPC) (3–5), EBV-associated gastric cancer, Burkitt's lymphoma, and Hodgkin's lymphoma (6–9). The viral oncogenic factors, such as RNA transcripts and proteins expressing during the latent or lytic phase have been reported to drive pathogenic processes (10, 11).

The EBV immediate-early protein BZLF1 is highly expressed following lytic stimuli induction, and it mediates the transition from the latent to the lytic replication cycle, which is critical for viral spread (12–15). As a transcription factor, BZLF1 binds to the promoters of many viral lytic genes as well as cellular genes to regulate their expression through EBV–host crosstalk (16). It has been reported that BZLF1 indirectly inhibits the expression of IFN-γ and promotes the expression of VEGF, IL10, and IL13 *via* viral proteins (10, 17). In addition, BZLF1 was also identified to directly regulate the expression of various host genes, such as FOSB and RASA3 (16).

Krüppel-like factor 4 (KLF4) is a zinc-finger transcription factor belonging to its eponymous family, which is implicated in cell growth, proliferation, and differentiation (18). Recently, there is increasing evidence that KLF4 is involved in other biological processes such as viral infection. For example, KLF4 negatively regulated cellular antiviral response by inhibiting the activation of NF-κB by TNF-α and IL-1β (19). In addition, melatonin was found to stabilize KLF4 by preventing its m^6A-dependent mRNA decay (20). However, whether and how KLF4 is regulated by the *N*6-methyladenosine (m^6A) modification *via* virus–host interaction need to be further elucidated.

m^6A is the most prevalent internal modification present in the messenger RNAs of eukaryotes viruses that replicate in the nucleus (21–24). The modification is introduced by a multicomponent "writer" complex consisting of the enzyme methyltransferase-like 3 (METTL3) and other cofactors including METTL14 and WTAP (25). The resulting m^6A residues are recognized by "reader" proteins such as YTHDF2 and YTHDF3, which contain a YTH domain that directly binds to m^6A (22, 26–28). There are multiple lines of evidence that m^6A plays an important role in regulating viral infection. Previous studies characterized the m^6A RNA methylomes of many RNA viruses, including human immunodeficiency virus, Zika virus, hepatitis C virus, enterovirus 71, murine leukemia virus, and the plant virus alfalfa mosaic virus (29–38), as well as numerous DNA viruses including hepatitis B virus, herpes simplex virus type 1, simian virus 40, Kaposi's sarcoma-

‡ These authors contributed equally to this work.
* For correspondence: Zhixiang Zuo, zuozhx@sysucc.org.cn; Tian-Liang Xia, xiatl@sysucc.org.cn.

© 2021 THE AUTHORS. Published by Elsevier Inc on behalf of American Society for Biochemistry and Molecular Biology. This is an open access article under the CC BY-NC-ND license (http://creativecommons.org/licenses/by-nc-nd/4.0/).

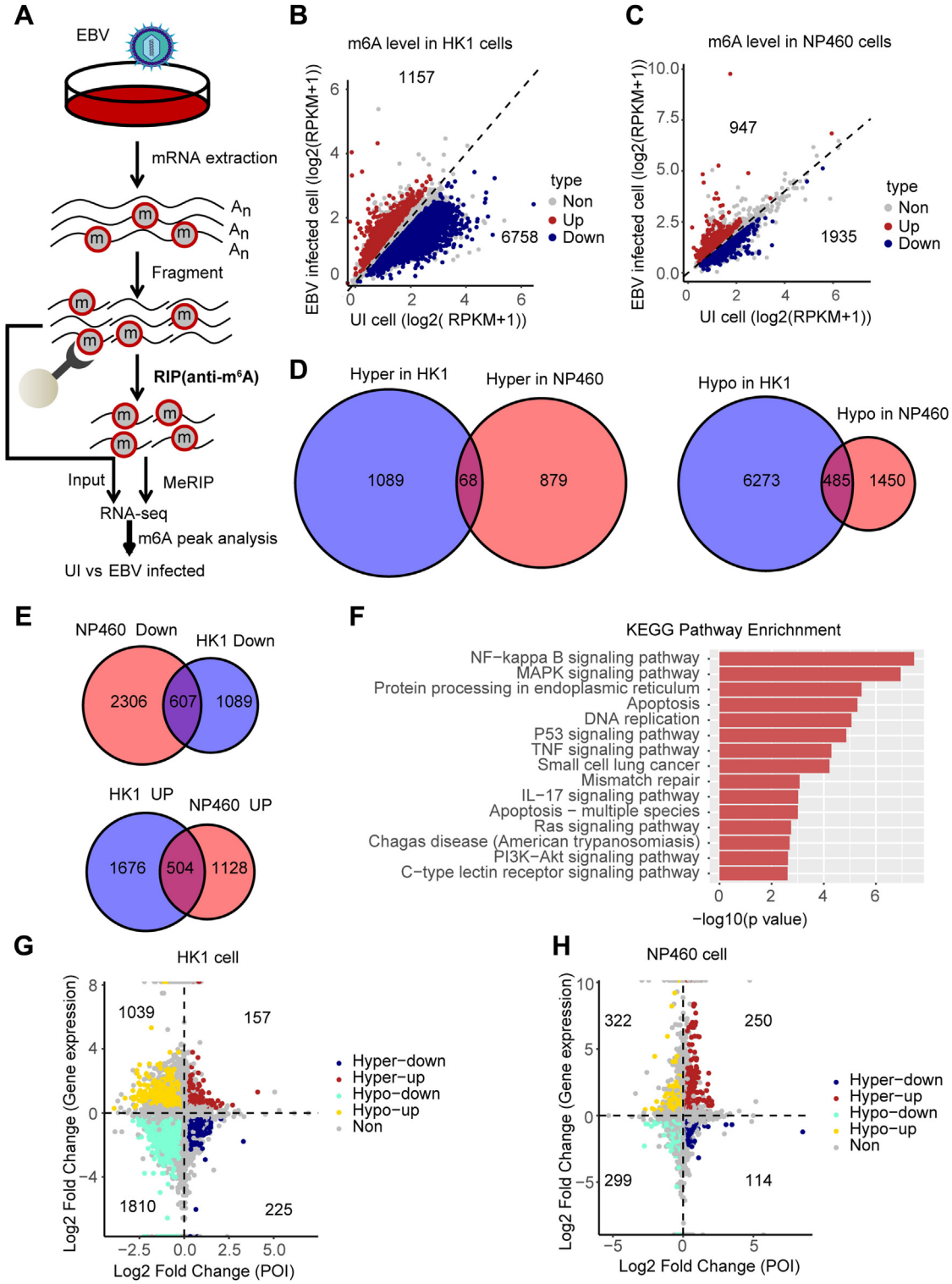

Figure 1. EBV infection alters m⁶A modification and RNA expression of host genes. *A*, schematic representation of the MeRIP-seq protocol used to identify differential m⁶A modification following infection of HK1 and NP460 cells with EBV-GFP. RNA was harvested at 24 h postinfection (hpi). *B* and *C*, the differential peaks (fold change ≥ 1.2) identified by MeRIP-seq in HK1 (*B*) and NP460 cells (*C*). RPKM, the mean RPKM value of two biological replicates of MeRIP-seq; Up, the peaks with upregulated m⁶A level in EBV-infected cells; Down, the peaks with downregulated m⁶A level; ns, not significant. *D*, the overlap results of the differential peaks in HK1 and NP460 cells from (*B*) and (*C*). *E*, the overlap results of the differential expression level of genes in HK1 and NP460 cells. *F*, the KEGG pathway enrichment results of the genes with differential expression level. *G* and *H*, distribution of the peaks with EBV-induced changes of m⁶A levels with differential gene expression in HK1 (*G*) and NP460 cells (*H*). Differential peaks, fold change ≥ 1.2; differential gene expression, fold change ≥ 1.2. Hyper-down, hypermethylated m⁶A genes with downregulated expression; Hyper-up, hypermethylated m⁶A genes with upregulated expression; Hypo-down, hypomethylated m⁶A genes with downregulated expression; Hypo-up, hypomethylated m⁶A genes with upregulated expression; Non, no difference; UI, uninfected sample.

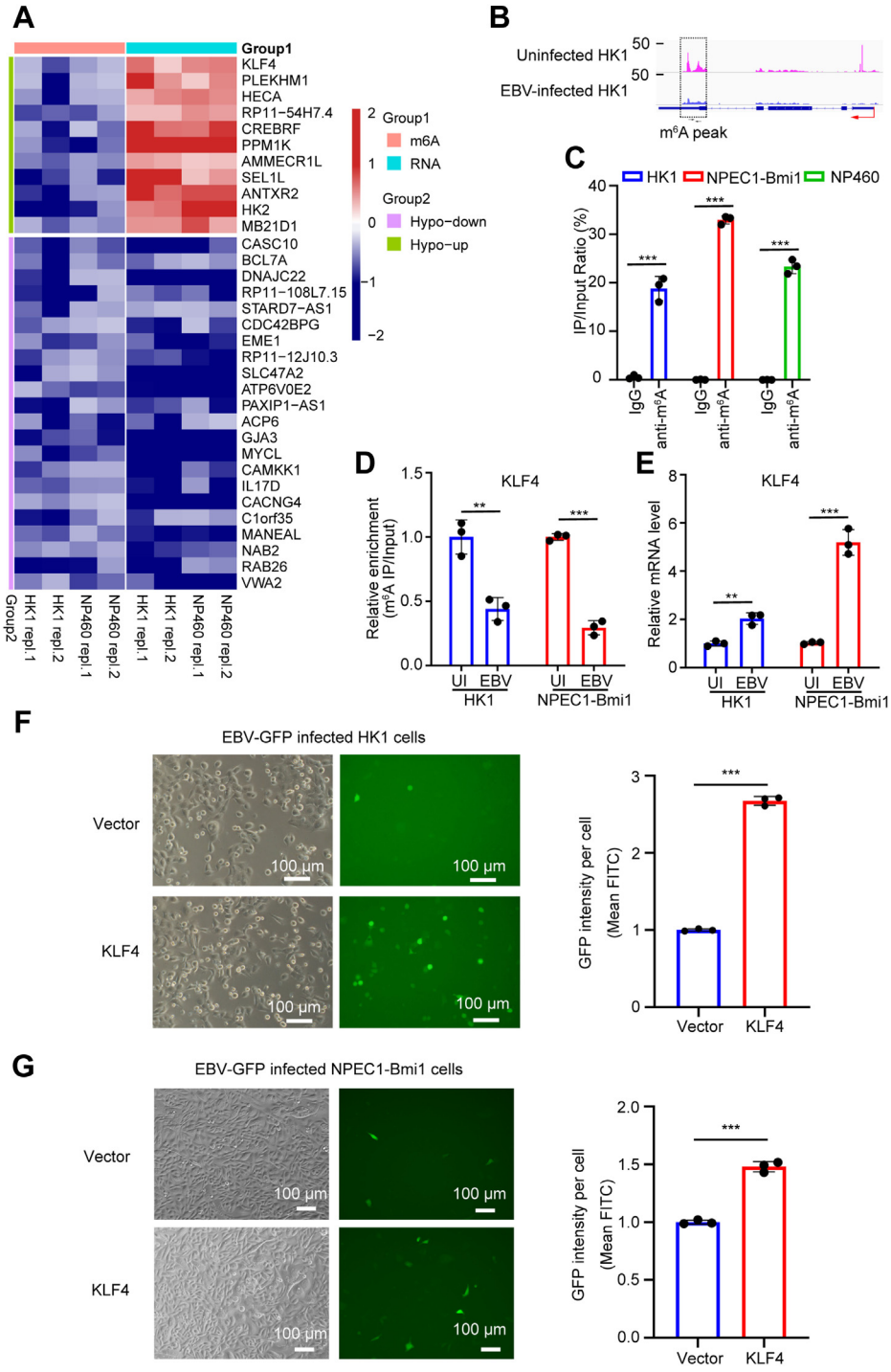

Figure 2. KLF4 promotes EBV infection as a hypo-up gene. *A*, the m^{6}A and expression levels of the hypo-up and hypo-down genes from the MeRIP-seq data. *B*, m^{6}A enrichment results of KLF4 by MeRIP-seq. The *box region*, m^{6}A peak of KLF4; *black arrows*, primers of KLF4; *red arrow*, transcription orientation of KLF4. *C*, the IgG or anti-m^{6}A antibody enrichment of KLF4 mRNA according to RIP-qPCR assay. The percentage of enriched KLF4 mRNA was determined by dividing IP by input. *D*, the m^{6}A level of KLF4 following the infection of HK1 and NPEC1-Bmi1 cells with EBV-GFP for 24 h. Fold enrichment was determined by dividing the fold change between the IP and the input, and the mean value of the m^{6}A level of KLF4 in the uninfected cells was defined as 1. *E*, the mRNA expression level of KLF4 following the infection of HK1 and NPEC1-Bmi1 cells with EBV-GFP for 24 h. The KLF4 mRNA expressions levels were normalized to the housekeeping gene ACTB. *F*, the effects of KLF4 overexpression in HK1 cells after EBV-GFP infection for 24 h were detected by fluorescence microscopy and FACS. *Left*, representative data from three independent experiments. Scale bars represent 100 μm. *Right*, quantification of the GFP-positive cells from three independent experiments. The GFP intensity per cell was determined by measuring the mean FITC value by FACS. The mean value of the GFP intensity per cell in the vector control cells was defined as 1. *G*, the effects of KLF4 overexpression in NPEC1-Bmi1 cells after EBV-GFP infection for 24 h were detected by fluorescence microscopy and FACS. *Left*, representative data from three independent experiments. Scale bars represent 100 μm. *Right*, quantification of the GFP-positive cells from three independent experiments. The GFP intensity per cell was determined by measuring the mean FITC value by FACS. The mean value of the GFP intensity per cell in the vector control cells was defined as 1. The shown datas represent as the means ± SD from three biological replicates. $^{**}p < 0.01$, $^{***}p < 0.001$ according to Student's *t*-test. EBV, EBV-GFP infected cells; UI, uninfected cells.

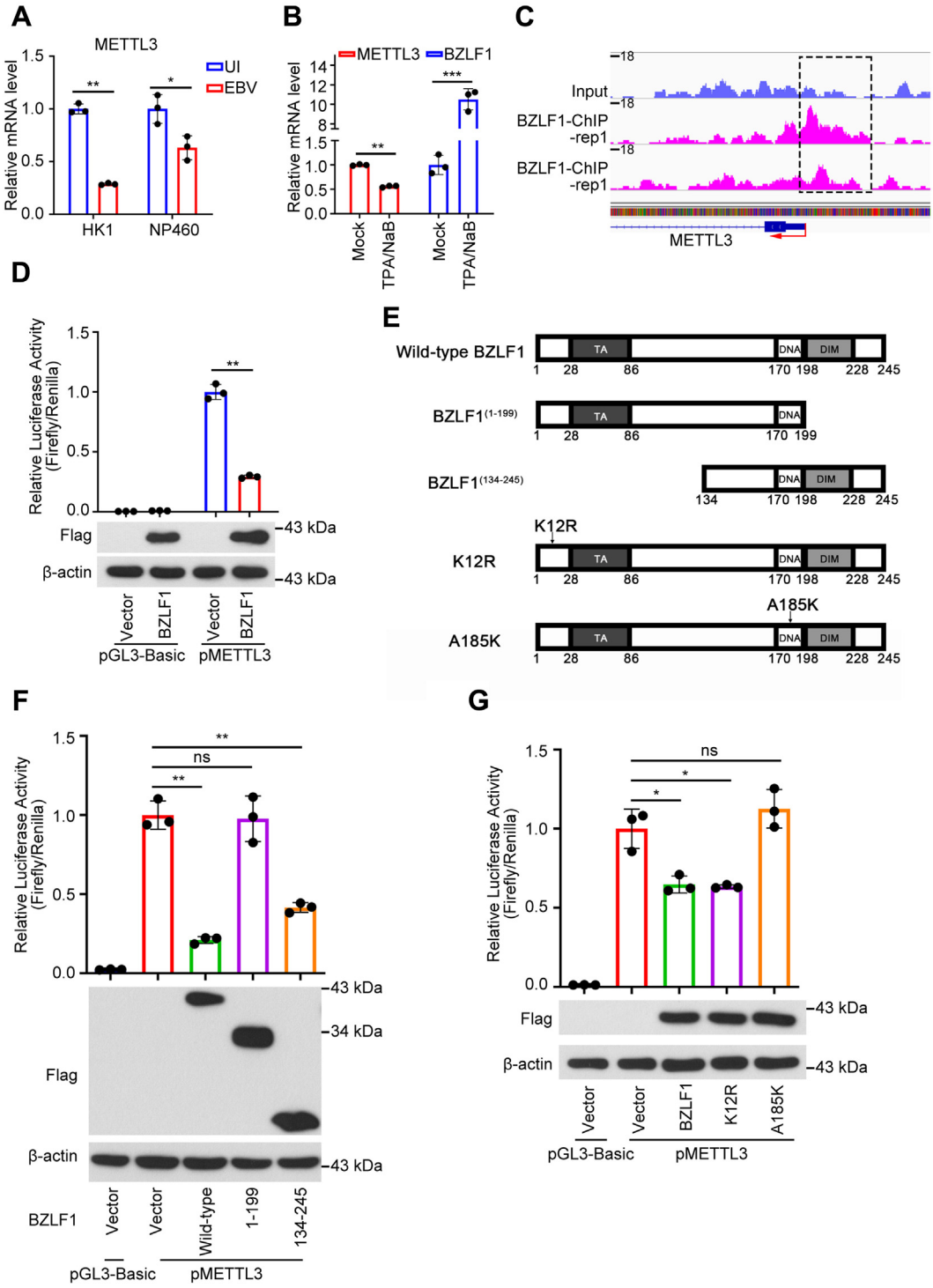

Figure 3. BZLF1 suppresses METTL3 promoter activity. *A*, the mRNA expression level of METTL3 following the infection of HK1 and NP460 cells with EBV-GFP for 24 h. The METTL3 mRNA expression level was normalized to the housekeeping gene ACTB. *B*, the mRNA expression levels of METTL3 and BZLF1 in CNE2EBV cells following the induction of EBV reactivation with TPA (30 ng/ml)/NaB (2 mM) treatment for 24 h. The METTL3 and BZLF1 mRNA expression levels were normalized to the housekeeping gene ACTB. *C*, the enrichment of METTL3 promoter using BZLF1 ChIP-seq from the GEO datasets (GSE83354, Input: GSM2200165; BZLF1-ChIP: GSM2200163 and GSM2200164) in HONE1 cells. *Red arrow*, transcription orientation of METTL3; *box region*, significant peak region of BZLF1 ChIP-seq. *D*, luciferase activity of the METTL3 promoter following the transfection of 293T cells with the indicated plasmids for 24 h. The promoter activity was determined by dividing the fold change between the firefly luciferase value and the Renilla luciferase value. The mean value of the METTL3 promoter activity in the vector control cells was defined as 1. The protein level of BZLF1 was analyzed by western blotting using an anti-Flag antibody with β-actin as loading control. *E*, schematic representation of the full-length BZLF1 protein, two truncation mutants, and two amino acid exchange mutation. A185K, alanine 185 mutated to lysine. *F*, the luciferase activity of METTL3 promoter following transfection of 293T cells for 24 h with indicated truncated mutant plasmids. The experiments were performed similarly as described (*D*) except for plasmid transfection. *G*, luciferase activity of METTL3 promoter following transfection of 293T cells for 24 h with the indicated plasmids encoding amino acid variants. The experiments were performed similarly as described for (*D*) except for plasmid transfection. The datas represent the means ± SD from three biological replicates. ns, not significant; *$p < 0.05$; **$p < 0.01$; ***$p < 0.001$ according to Student's *t*-test. DIM, dimerization bZIP domain; DNA, basic DNA binding region; EBV, EBV-GFP infected cells; K12R, lysine 12 mutated to arginine; pMETTL3, the METTL3 promoter in the pGL3-basic plasmid; TA, transactivation domain; UI, uninfected cells.

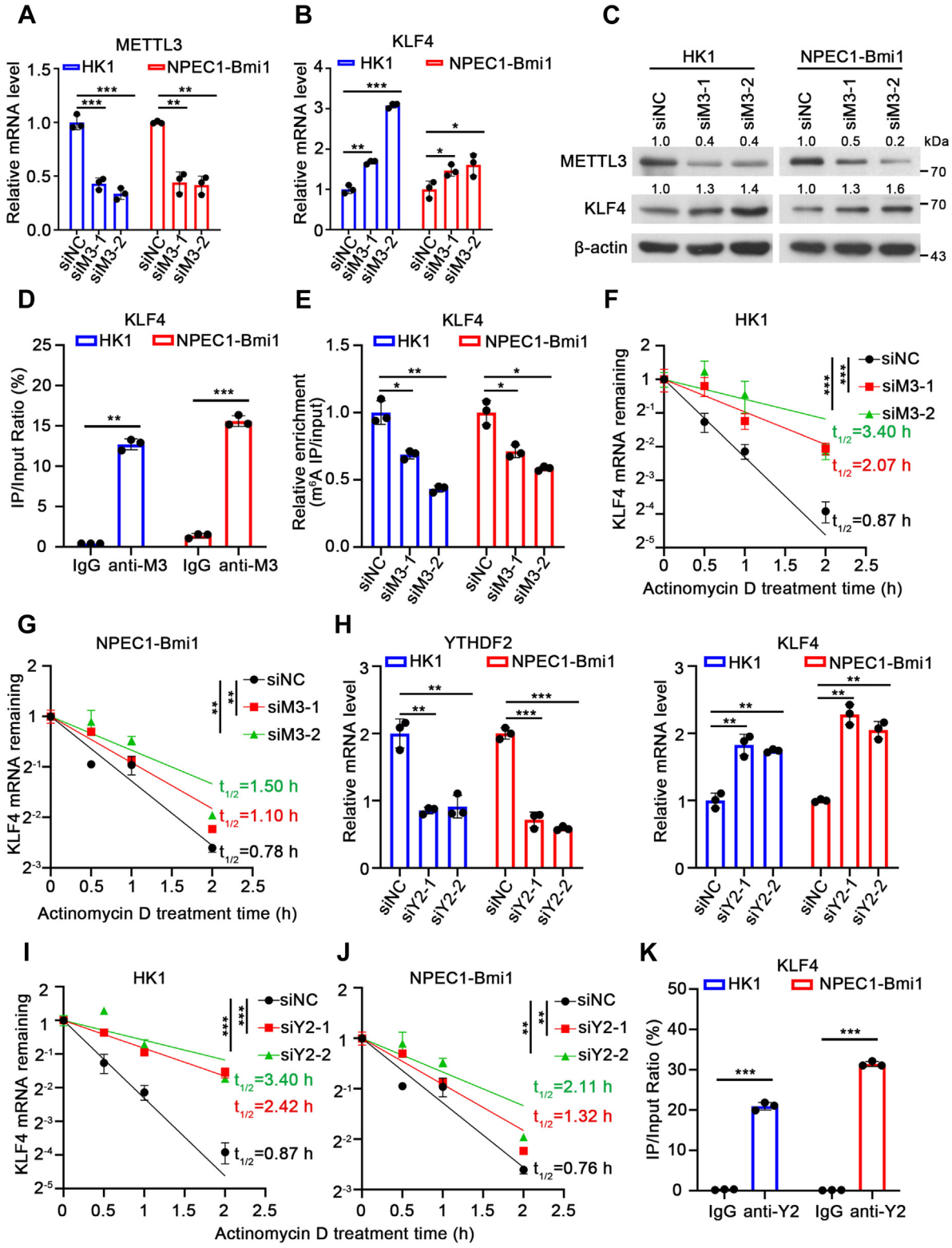

Figure 4. METTL3 and YTHDF2 accelerate the mRNA decay of the cellular gene KLF4. *A* and *B*, METTL3 (*A*) and KLF4 (*B*) mRNA levels in HK1 and NPEC1-Bmi1 cells transfected with METTL3-specific siRNAs (siM3-1 or siM3-2) for 24 h. At 24 h post-siRNA transfection, the knockdown efficiency of METTL3 (*A*) and the KLF4 mRNA level (*B*) were determined by qRT-PCR. The mRNA expression levels were normalized to the housekeeping gene ACTB. *C*, METTL3 and KLF4 protein level in HK1 and NPEC1-Bmi1 cells transfected with METTL3-specific siRNAs (siM3-1 or siM3-2) for 24 h were analyzed by western blotting with β-actin as the loading control. The numbers represent the ratio of band intensity of KLF4/β-actin and METTL3/β-actin. *D*, the relative METTL3-RIP enrichment of the KLF4 mRNA was analyzed by RIP-qPCR in HK1 and NPEC1-Bmi1 cells. The percentage of enriched KLF4 mRNA was determined by dividing IP by input. IgG was used as control. *E*, the relative m^{6}A enrichment of KLF4 mRNA in HK1 cells transfected with METTL3-specific siRNAs for 24 h. Fold enrichment was determined by dividing the fold change of the IP and the input, and the value of the m^{6}A level of KLF4 in the control siRNA transfected cells was defined as 1. *F* and *G*, increasing the half-life of KLF4 mRNA by knockdown of METTL3 in HK1 (*F*) and NPEC1-Bmi1 (*G*) cells. The remaining mRNA levels of KLF4 after actinomycin D (2 μg/ml) treatment in METTL3 knockdown or siNC control HK1 cells. The results were normalized to the relative mRNA level at 0 h after the

associated herpesvirus, and EBV (39–46). Viral infection alters the cellular m⁶A modification level to regulate different biological processes (32, 40, 42, 47). Recently, the role of m⁶A in EBV-associated tumorigenesis has been investigated by Lang *et al.* (44), who examined the viral epitranscriptome of EBV-transformed cell lines.

Here, we focused on the modification of cellular genes upon EBV infection in nasopharyngeal cells. We found that EBV infection decreased the METTL3-mediated m⁶A modification of the host gene KLF4, thereby increasing its expression to promote EBV infection. Mechanistically, the expression of METTL3 was inhibited by BZLF1 during viral infection, which increased the mRNA stability of KLF4. Overall, our results demonstrated a positive feedback loop between BZLF1 and KLF4 that facilitated EBV infection, providing new insights into the crosstalk between virus and host cell.

Results

EBV infection alters RNA m⁶A modification and expression of host genes

Previous studies found that viral infection alters the m⁶A modification of host genes (32, 40, 42, 48). To identify the m⁶A modification changes in cellular mRNAs following EBV infection, we performed immunoprecipitation and sequencing of methylated RNA (MeRIP-seq) in infected and uninfected nasopharyngeal epithelial cells (Fig. 1*A*). After extracting the mRNA from NP460 and HK1 cells at 24 h postinfection with EBV, we used an anti-m⁶A antibody to enrich m⁶A-modified RNA fragments. This was followed by RNA sequencing of both the input and immunoprecipitated fractions. A significant number of cellular genes with altered m⁶A modification in response to EBV infection were screened out. As indicated, 25,902 m⁶A peaks spanning on 11,601 cellular genes in HK1 cells, as well as 27,007 m⁶A peaks spanning on 12,110 cellular genes in NP460 cells, were identified (Tables S1 and S2). In total, 6758 peaks were downregulated and 1157 peaks were upregulated in HK1 cells (Fig. 1*B*). In total, 1935 peaks were downregulated and 947 peaks were upregulated in NP460 cells (Fig. 1*C*). Among these, 553 differential peaks were present in both cell lines (fold change $\geqq$ 1.2), 68 of which showed increased m⁶A levels, while 485 showed decreased m⁶A levels, termed as hyper- and hypomethylated peaks, respectively (Fig. 1*D*). Almost 87% of the altered m⁶A peaks were hypomethylated, indicating that the m⁶A levels of total mRNAs of the host were impaired upon viral infection. To verify this hypothesis, we used a cellular RNA m⁶A level quantification kit to assess the m⁶A level of EBV-infected HK1, NP460, and NPEC1-Bmil cells. As expected, the m⁶A levels of cellular genes were lower in the EBV-infected cells (Fig. S1). Next, the hypomethylated genes were screened out for further analysis combined with the differential gene expression.

As for the differential gene expression, a total of 607 genes were downregulated and 504 were upregulated following EBV infection in HK1 and NP460 cells (Fig. 1*E*). KEGG pathway analysis indicated that these genes were mainly enriched in the NF-κB signaling pathway (Fig. 1*F*), which was consistent with a previous report that viral infection primarily triggered the activation of the transcription factors NF-κB and IRF3 to elicit antiviral response (19). Combined analysis of the m⁶A levels and differential gene expression revealed 3231 and 985 differential peaks in the EBV-infected HK1 cells and NP460 cells, respectively (Fig. 1, *G* and *H* and Tables S1 and S2).

Taken together, the results indicated that EBV infection not only decreased cellular m⁶A modification, but also regulated the mRNA levels of cellular genes which was mainly related to the NF-κB pathway. We therefore set out to further elucidate the crucial genes participating in the regulation.

EBV infection reduces the mRNA m⁶A modification level of KLF4 and enhances its expression

After overlap analysis of the differential expression genes with m⁶A hypomethylated in both EBV infected cells, the MeRIP-seq data revealed that 33 hypomethylated genes were differentially expressed following EBV infection (Fig. 2*A*). Among these genes, KLF4, a transcriptional regulator of the NF-κB signaling pathway, has been reported to induce lytic EBV reactivation in Burkitt lymphoma cells (49, 50). As indicated in our MeRIP-seq data, KLF4 exhibited lower m⁶A modification and higher expression levels in the context of EBV infection. Furthermore, EBV infection decreased the m⁶A levels in the KLF4 mRNA (Fig. 2*B*), indicating that it may be modified and regulated by EBV.

Next, RIP assays were performed using an anti-m⁶A antibody or IgG control. The results indicated that KLF4 was highly m⁶A-modified in HK1, NPEC1-Bmi1, and NP460 cells (Fig. 2*C*). To determine the role of KLF4, we performed MeRIP and qRT-PCR assays to measure its m⁶A modification and expression levels in EBV infected HK1 and NPEC1-Bmi1 cells. As indicated, the m⁶A modification level of KLF4 was downregulated in response to viral infection, accompanied by increased expression of KLF4 (Fig. 2, *D* and *E*). To further validate the role of KLF4 in EBV infection, we transfected HK1 and NPEC1-Bmi1 cells with a KLF4 plasmid, followed by EBV-GFP infection. The fluorescence microscopy and flow cytometry results revealed that nasopharyngeal epithelial cells with

Actinomycin D treatment. The datas represent the means ± SD from three biological replicates. Half-lives ($t_{1/2}$) were obtained from linear regression analysis. Significance was assesses using two-way ANOVA; $^{**}p < 0.01$, $^{***}p < 0.001$. *H*, YTHDF2 and KLF4 mRNA levels in HK1 and NPEC1-Bmi1 cells transfected with YTHDF2-specific siRNAs (siY2-1 or siY2-2) for 24 h. The knockdown efficiency of YTHDF2 was determined by qRT-PCR. The mRNA expression levels were normalized to the housekeeping gene ACTB. *I* and *J*, increasing the half-life of KLF4 mRNA by knockdown of YTHDF2 in HK1 (*I*) and NPEC1-Bmi1 (*J*) cells. The experiments were performed similarly as described for (*F*) except for the siRNA transfection. The datas represent the means ± SD from three biological replicates. Significance was assessed using two-way ANOVA, $^{**}p < 0.01$, $^{***}p < 0.001$. *K*, the relative YTHDF2-RIP enrichment of the KLF4 mRNA was analyzed by RIP-qPCR in HK1 and NPEC1-Bmi1 cells. The percentage of enriched KLF4 mRNA was determined by dividing the fold change of IP and the input. IgG was used as control. The datas from *A*, *B*, *D*, *E*, *H*, and *K* represent the means ± SD from three biological replicates. $^{*}p < 0.05$; $^{**}p < 0.01$; $^{***}p < 0.001$; according to Student's *t*-test.

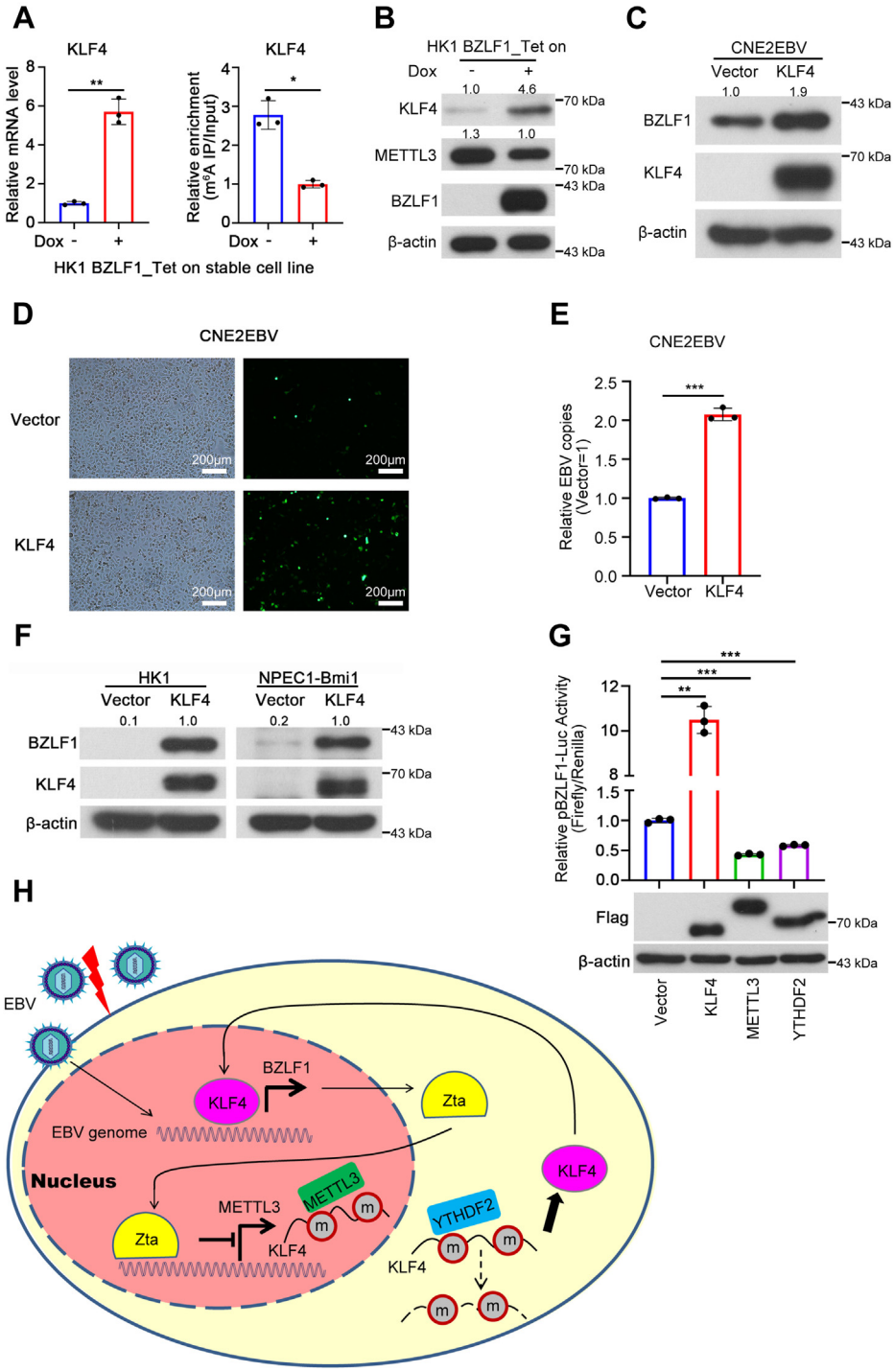

Figure 5. KLF4 promotes the expression of BZLF1 and enhances the lytic replication of EBV. *A*, the mRNA and the m^{6}A levels of KLF4 following BZLF1 overexpression in HK1 cells. The total RNA was extracted at 24 h post doxycycline (1 μg/ml) treatment. The RNA levels were analyzed by qPCR and the m^{6}A level by MeRIP-qPCR. *B*, the protein expression levels of KLF4, METTL3, and BZLF1 in BZLF1-overexpressed HK1 cells were analyzed by western blotting with β-actin as loading control. The proteins were harvested at 24 h post doxycycline treatment. The numbers represent the ratios of the band intensities of KLF4/β-actin and METTL3/β-actin. *C*, BZLF1 protein levels in CNE2EBV cells transected with KLF4 or vector control for 24 h. Beta-actin was used as loading control. The numbers represent the ratios of the band intensities of BZLF1/β-actin. *D*, the effects of KLF4 overexpression in CNE2EBV cells were detected by fluorescence microscopy. The images show representative data from three independent experiments. Scale bars represent 200 μm. *E*, the average number of EBV copies in CNE2EBV cells with transfected with KLF4 or vector control for 24 h. The EBV copy numbers were detected using qPCR with a specific primer targeting the EBV BALF5 gene region, and GAPDH was used as a reference genome copy. *F*, BZLF1 protein expression in KLF4 overexpressed HK1 and NPEC1-Bmi1 cells was analyzed by western blotting after acute infection with EBV-GFP for 24 h. At 24 h post transfection of KLF4 or vector control, the cells were infected with EBV-GFP for 24 h. Beta-actin was used as loading control. The numbers represent the ratio of the band intensities in BZLF1/β-actin. *G*, the promoter activity of BZLF1 in 293T cells transfected with the indicated plasmids for 24 h. The BZLF1 promoter activity was determined by dividing the fold change of the firefly luciferase value with the Renilla luciferase value, and the mean value of the BZLF1 promoter activity in the vector control cells was defined as 1. The protein levels of KLF4, METTL3, and YTHDF2 were analyzed by western blotting using an anti-Flag antibody. Beta-actin was used as loading control. *H*, a working model for the crosstalk between EBV and host cells. After EBV acute infection, the EBV IE gene BZLF1 was immediately expressed and suppressed the expression of the m^{6}A modification writer METTL3 to regulate cellular m^{6}A levels. Lower expression of METTL3 could increase the RNA

higher expression of KLF4 were more susceptible to acute EBV infection, as revealed by their higher fluorescence ratio (Fig. 2, *F* and *G*).

Overall, EBV infection reduced the m^{6}A modification of KLF4 and increased its expression, which promoted the EBV infection of nasopharyngeal epithelial cells. We next investigated the mechanism underlying the EBV-induced decrease of KLF4 m^{6}A modification.

EBV infection reduces the expression of METTL3

Since METTL3 is the key enzyme in the m^{6}A writer complex, we next sought to determine whether EBV infection affected the expression level of METTL3. As predicted, the mRNA level of METTL3 was significantly downregulated in HK1 and NP460 cells after EBV infection (Fig. 3*A*). It has been reported that EBV can be reactivated by 12-O-tetradecanoylphorbol-13-acetate (TPA) and sodium butyrate (NaB) (51–54). Consistently, the expression of METTL3 was reduced after induction of lytic virus replication in CNE2EBV cells by TPA/NaB treatment, while expression of BZLF1 was increased (Fig. 3*B*). Mounting evidence supports the idea that BZLF1 is the major transcription factor regulating numerous viral and cellular genes in response to EBV infection. BZLF1 is not only a transcriptional activator, but also as a repressor (13, 55–57). We therefore hypothesized that BZLF1 might regulate the promoter activity of METTL3. By analyzing the BZLF1 ChIP-seq data in the NPC cell line HONE1 (58) from the GEO datasets, we found that BZLF1 interacted with the promoter of METTL3 (Fig. 3*C*). To further verify this result, we constructed a luciferase reporter driven by METTL3 promoter and the luciferase assay indicated that overexpression of BZLF1 dramatically inhibited the promoter activity of METTL3 (Fig. 3*D*).

To understand which domains of BZLF1 mediate the repression of the METTL3 promoter, we generated the truncated variants BZLF1$^{(1\text{-}199)}$ and BZLF1$^{(134\text{-}245)}$ for the luciferase assay (Fig. 3*E*). The BZLF1$^{(1\text{-}199)}$ truncation could not form dimers due to a deletion of the C-terminal dimerization domain (59, 60). The BZLF1$^{(134\text{-}245)}$ truncation lacks the N-terminal transactivation domain and could not trans-activate a reporter construct (13). A recent study found that BZLF1 suppressed the expression of the host gene CIITA's *via* a mechanism that was independent of dimerization and DNA binding of BZLF1 (57). However, our result indicated that it was BZLF1$^{(134\text{-}245)}$ truncation, relying on the dimerization domain, that suppressed the promoter activity of METTL3 and not the BZLF1$^{(1\text{-}199)}$ variant (Fig. 3*F*). The dimerization domain of BZLF1 therefore enables it to suppress METTL3 promoter activity.

There is increasing evidence that sumoylation and DNA-binding activity of BZLF1 are important for regulating cellular genes (61). To further investigate whether the transcriptional repression of the METTL3 promoter by BZLF1 was related to its sumoylation or DNA-binding activity, we generated the BZLF1 (K12R) variant carrying a sumoylation site mutation (61) and the BZLF1 (A185K) variant bearing a binding site mutation (17, 55) for further luciferase assays (Fig. 3*E*). The K12R mutation did not affect the transcriptional repression activity of BZLF1 at the METTL3 promoter (Fig. 3*G*), which was consistent with our previous finding that the repression of METTL3 by BZLF1 is independent of its N terminal (Fig. 3*F*). By contrast, the BZLF1 (A185K) mutant did not exhibit any transcriptional suppression activity at the METTL3 promoter (Fig. 3*G*), indicating that BZLF1 suppressed METTL3 promoter activity based on DNA-binding activity.

Collectively, our results suggested that BZLF1, a transcription factor that was highly expressed during EBV infection, bound the promoter of METTL3 to suppress its expression and that this transcriptional suppression activity is dependent on the dimerization domain and DNA-binding activity of BZLF1.

METTL3 and YTHDF2 accelerate the mRNA decay of KLF4

Since we found that EBV infection suppressed the expression of METTL3 and promoted the expression of KLF4, we wondered whether METTL3 plays a role in regulating the expression of KLF4. We transfected HK1 and NPEC1-Bmi1 cells with two individual METTL3-specific siRNAs and verified the knockdown efficiency (Fig. 4*A*). Knockdown of METTL3 markedly increased the expression of KLF4 at both the mRNA and protein levels (Fig. 4, *B* and *C*). Consistently, overexpression of METTL3 decreased the expression of KLF4 (Fig. S2*A*). A RIP assay also revealed that METTL3 interacted with the transcripts of KLF4 in HK1 and NPEC-Bmi1 cells (Fig. 4*D*). Knockdown of METTL3 decreased the m^{6}A modification level of the KLF4 transcript (Fig. 4*E*), which was consistent with the finding that EBV infection impaired the m^{6}A modification of KLF4 (Fig. 2, *D* and *E*). Since it has been reported that the m^{6}A modification level regulates the decay of mRNA, we hypothesized that METTL3 might regulate the decay of KLF4 to affect its expression through m^{6}A modification. HK1 cells with METTL3 knockdown were treated with actinomycin D, which inhibits the transcription of cellular gene transcription in a time-dependent manner. Subsequent qRT-PCR analysis indicated that the mRNA decay of KLF4 was slowed down in cells with METTL3 knockdown compared with the control cells (Fig. 4, *F* and *G*). Thus, METTL3 modified the KLF4 mRNA and promoted its decay.

There is increasing evidence that the m^{6}A writer YTHDF2 participates in the regulation of mRNA degradation (27). To understand the role of YTHDF2 in regulating the expression of KLF4, we used two YTHDF2-targeting siRNAs with confirmed knockdown efficiency (Fig. 4*H*). As expected, the mRNA level of KLF4 was significantly increased when YTHDF2 was knocked down (Fig. 4*H*). Moreover, knockdown of YTHDF2 inhibited the decay of the KLF4 mRNA (Fig. 4, *I* and *J*). A RIP

stability of KLF4, one of the altered m^{6}A modified cellular genes, by protecting it from YTHDF2-mediated RNA decay. KLF4 could in turn increase BZLF1 transcription to promote lytic EBV infection of nasopharyngeal epithelial cells. The datas represent the means ± SD from three biological replicates. $^{**}p < 0.01$; $^{***}p < 0.001$, according to Student's *t*-test.

assay was conducted to detect the association between YTHDF2 and KLF4, and it confirmed that they interacted in both HK1 and NPEC-Bmi1 cells (Fig. 4*K*).

These result indicated that METTL3 and YTHDF2 accelerated the mRNA decay of KLF4 by increasing the m^{6}A modification level.

KLF4 promotes the expression of BZLF1 and enhances the lytic replication of EBV

Since EBV infection inhibited the expression of KLF4, we reasoned that BZLF1 may act as a viral transcription regulator that controls KLF4. To test this hypothesis, we generated a stable cell line expressing the BZLF1 gene. The mRNA and protein level of KLF4 were significantly increased in cells with increased expression of BZLF1 following DOX treatment, whereas the level of m^{6}A modified KLF4 was reduced significantly, accompanied by a decrease of the METTL3 expression level (Fig. 5, *A* and *B*).

Next, we sought to determine whether KLF4 also regulated the expression of BZLF1. As reported, KLF4 could regulate EBV infection in telomerase-immortalized normal oral keratinocyte epithelial cells by promoting the transcription of the EBV IE gene, BZLF1 (49). Here, we also found that the overexpression of KLF4 promoted the expression of BZLF1 in HK1EBV and CNE2EBV cells persistently carrying EBV-GFP (Figs. 5*C* and S3*A*), resulting in stronger fluorescence intensity of EBV-GFP undergoing lytic replication (Figs. 5*D* and S3*B*). The qPCR results indicated that the EBV lytic copy number increased twofold in KLF4 overexpressing CNE2EBV cells (Fig. 5*E*), as well as 1.5-fold in HK1EBV cells, compared to vector control cells (Fig. S3*C*). Furthermore, overexpression of KLF4 promoted the expression of BZLF1 upon EBV acute infection (Fig. 5*F*), leading to higher EBV infection efficiency (Fig. 2, *F* and *G*). In addition, we found that overexpression of KLF4 significantly increased the promoter activity of BZLF1, while overexpression of METTL3 and YTHDF2 had the opposite effect (Fig. 5*G*). Thus, KLF4 could promote EBV lytic replication by upregulating the expression of BZLF1, which was inhibited by METTL3 and YTHDF2 *via* m^{6}A modification.

Based on the results, we proposed a working model for the crosstalk between EBV and host cells (Fig. 5*H*). After EBV acute infection, the EBV IE protein BZLF1 was highly expressed and suppressed the expression of the m^{6}A writer METTL3 by interacting with its promoter. The reduced expression of METTL3 suppressed the m^{6}A modification of KLF4, which increased the RNA stability of KLF4 by reducing m^{6}A modification reader YTHDF2-mediated mRNA decay. In return, the higher expression of KLF4 promoted EBV lytic infection in epithelial cells. Thus, the BZLF1 and KLF4 serve as a feedback loop to promote EBV infection of the host through crosstalk with METTL3 and YTHDF2.

Discussion

Several recent studies found that viral infection could alter the cellular m^{6}A levels through various pathways. For example, the HIV-1 envelope protein gp120 upregulated the m^{6}A levels of cellular RNAs independently of viral replication (47). Similarly, EV71 and HCMV infection was found to upregulate the expression of the m^{6}A writers METTL3 and METTL14 (37, 62, 63). Previously, Lang *et al.* (48) had found that lytic reactivation of EBV infection could suppress the expression of the m^{6}A writer METTL14 in LcL, Akata, 293T-EBV, Mutu I, and Mutu III cells. In this study, we found that EBV infection decreased METTL3 expression in nasopharyngeal epithelial cells *via* the viral transcription factor BZLF1. Interestingly, the cellular m^{6}A modification could in turn influence the virus infection. A recent study found that changes in the m^{6}A modification of the cellular mRNAs RIOK3 and CIRBP influenced their translation and splicing, which subsequently affected flaviviridae infection. Here, we found that EBV infection increased the expression of KLF4 by downregulating the m^{6}A modification of its mRNA, which ultimately promoted EBV infection of the host.

It has been reported that KLF4 is a transcription factor with roles in the cell proliferation, apoptosis, and differentiation (18). KLF4 was also known for its ability to convert differentiated cells into IPS cells together with other transcriptional factors (49). However, little is known about the role of m^{6}A modification of KLF4 upon viral infection. Here, we found that the m^{6}A modification of KLF4 was inhibited by decreased METTL3 expression in response to EBV infection. A previous study found that KLF4 directly interacted with the promoter of BZLF1 to induce its expression and promoted lytic EBV infection (49), but the influence of BZLF1 on the regulation of KLF4 remained unexplored. Here, we found that BZLF1 interacted with the promoter of METTL3 to reduce its expression, which slowed down the mRNA decay of KLF4. Another study suggested that KLF4 can inhibit the recruitment of IRF3 to the IFNβ promoter by directly binding to it, thus inhibiting the activation of NF-κB by TNF-α and IL-1β (19). Based on these findings, we further hypothesized that KLF4 is upregulated during EBV infection and then not only binds to the promoter of the cellular IFNβ gene to repress immune responses, but also binds to the promoter of viral BZLF1 gene to boost its production, which synergistically further facilitate EBV infection.

BZLF1 has been identified as a transcriptional activator of many genes, including almost all lytic genes of EBV (13). However, studies found that BZLF1 also suppressed the expression of several genes, such as TNFR1, TAP2, and CIITA (55–57). The suppression of CIITA expression and TAP2 promoter activity was found to be dependent on the BZLF1 transcription domain, while the inhibition of TNFR1 promoter activity was dependent on BZLF1 transcription domain and DNA-binding domain. By contrast, the transcriptional repression of HADC3 mediated by sumoylation of BZLF1 protein required the transcriptional activation domain (61). Previous results therefore indicated that the transcriptional activation domain is crucial for the transcriptional suppression activity of BZLF1, without focusing on the importance of the dimerization domain and DNA-binding activity of BZLF1. However, our luciferase assay results indicated that BZLF1

bound to the promoter of METTL3 to suppress its expression, depending on its dimerization domain and DNA-binding activity rather than its transcription activation domain. The detailed mechanism of the transcriptional suppressor function of BZLF1 merits further investigation.

In summary, we provide solid evidence that m^{6}A modification is involved in the crosstalk between EBV and host cells *via* a positive feedback loop comprising the viral protein BZLF1, the m^{6}A writer METTL3, and the cellular gene KLF4. The detailed mechanisms through which the feedback loop is regulated must be explored further to gain a comprehensive understanding of EBV infection and the role of m^{6}A modification. These findings contribute to our understanding of the role of EBV-induced m^{6}A modification in virus–host interactions and may in turn further advance the development of prophylactic or curative therapies for EBV-associated diseases.

Experimental procedures

Cells and culture conditions

The 293T cell (ATCC, CRL-3216) was purchased from the American Type Culture Collection (ATCC). Bmi1-immortalized primary NPECs (NPEC1-Bmi1) were established in our laboratory as described previously (Life Technology) (64, 65). NPEC1-Bmi1 and NP460 cells were grown in keratinocyte serum-free medium (Life Technology). HK1 cells were grown in RPMI 1640 medium supplemented with 10% fetal bovine serum (FBS, GIBCO) and were a kind gift from Professor Quentin Liu (Sun Yat-sen University, Guangzhou, China) (66). EBV-positive AKATA cells, grown in RPMI 1640 medium supplemented with 5% FBS, were a kind gift from Professor Maria G. Masucci (Karolinska Institute, Sweden). CNE2EBV and HK1EBV cells were cultured in RPMI 1640 medium supplemented with 5% FBS and 500 μg/ml G418. The 293T cells were grown in Dulbecco's Modified Eagle's Medium supplemented with 10% fetal bovine serum.

EBV-GFP preparation and infection

EBV (Akata strain) with an integrated EGFP gene (EBV-GFP) was prepared in AKATA cells as described previously (64, 67). Briefly, EBV-GFP was produced in AKATA cells by reactivation with 0.8% (v/v) of a goat-anti-human IgG (Huayang Zhenglong Biochem Lab). After 72 h post EBV reactivation, the EBV-GFP was harvested and stored at −80 °C. Epithelial cells were exposed to EBV-GFP for 3 h at 37 °C, and the unbound virus was removed by washing twice with Hanks' solution. The infected cells were cultured in fresh medium for 24 h, followed by the quantification of GFP-positive cells *via* flow cytometry (Beckman Coulter FC500) and fluorescence microscopy.

Reagents

The antibodies used in this study were as follows: anti-BZLF1 (sc53904, Santa cruz, WB); anti-β-actin (66009-1-Ig, Proteintech, WB); anti-Flag-tag (F4049, Sigma, WB); anti-METTL3 (ab195352, Abcam, WB); anti-KLF4 (11880-1-AP, Proteintech, WB); horseradish peroxidase (HRP)-conjugated goat-anti-mouse/rabbit secondary antibodies (#31460, #61-6520, Invitrogen, WB); anti-METTL3 (15073-1-AP, Proteintech, RIP); anti-YTHDF2 (24744-1-AP, Proteintech, RIP). Reagent included actinomycin D (A9415, Sigma); TRIzol (T924, Sigma); and doxycycline (631311, TAKARA).

Plasmids

The METTL3 promoter (−861 to +13 from the transcription start site) and the BZLF1 promoter (−668 to +15) were PCR-amplified using specific primers with an Xho1 restriction enzyme site at the 5′-end and a Hind III site at the 3′-end. The promoters were subcloned into the pGL3-Basic plasmid. Flag-tagged BZLF1 was expressed using the pcDNA3.1+ vector. The expression vectors for Flag-BZLF1 (K12R) and Flag-BZLF1 (S185K) were generated by site-directed mutagenesis of Flag-BZLF1-pcDNA3.1+. The expression plasmids for Flag-BZLF1 $^{(134\text{-}245)}$ and Flag-BZLF1 $^{(1\text{-}199)}$ were generated from the Flag-BZLF1 plasmid by PCR. The pENTER plasmid and pENTER plasmids with flag tagged METTL3, YTHDF2, or KLF4 were purchased from Vigene Biosciences. To generate BZLF1 overexpressing cell lines, the Flag-BZLF1 coding sequence was PCR-amplified and inserted into pRetroX-TRE3G vector. To generate METTL3-overexpressing cell lines, the Flag-METTL3 coding sequence was PCR-amplified from Flag-METTL3-pENTER and then inserted into the pLVX-dsred-monomer-N1 vector.

Establishment of stable cell lines

The 293FT cells were transfected with the Flag-METTL3-pLVX-dsred-monomer-N1 plasmid or vector control using the packaging plasmids psPAX2 and pMD2G. The transfected cells were incubated at 37 °C for 6 h, after which the medium was replaced with fresh medium. Cell supernatants containing the viral particles were harvested at 48 h after the transfection. HK1 cells were stably transfected with the lentivirus and selected with puromycin (1 μg/ml).

The GP2-293 cells were transfected with the pRetroX-Tet3G or Flag-BZLF1-pRetroX-TRE3G plasmids using the packaging plasmid pVSV-G. Cell supernatants containing the viral particles were harvested at 48 h after transfection. HK1 cells were stably transfected with the retrovirus mixture of Tet3G and Flag-BZLF1-TRE3G and were selected with neomycin (200 μg/ml) and puromycin (1 μg/ml). The stable cell lines were treated with doxycycline at a final concentration of 1 μg/ml to induce Flag-BZLF1 expression. The stably overexpressing cell lines were then identified using qRT-PCR and western blot analysis.

MeRIP-seq and MeRIP-qPCR

The total RNA was isolated using the TRIzol reagent, and the mRNA was purified using the GenEluteTM mRNA Miniprep Kit (MRN10, Sigma). The mRNA was fragmented using the Ambion RNA Fragmentation Reagent (AM8740, Life Technologies) and then purified by ethanol precipitation. Then, 1/10 of fragmented RNA was retained as input for RNA sequencing. For MeRIP, the fragmented RNA was incubated with an anti-m^{6}A antibody (#202003, Synaptic Systems) conjugated to

ASBMB

Protein G Dynabeads (Thermo Fisher Scientific) in MeRIP Buffer. Unbound RNA was removed using a magnetic separator and the beads were washed five times with MeRIP buffer. The MeRIP RNA was then extracted with TRIzol. The sequencing of the input RNA samples and MeRIP samples was performed by RIBOBIO. STAR was used for reads mapping and MACS2 was used for m^{6}A peak calling (68, 69). The RNA-seq reads were normalized using the RSEM method (70).

The m^{6}A modification levels of KLF4 were determined using a MeRIP-qPCR assay. After the MeRIP assay, all input samples and MeRIP samples were subjected to qRT-PCR. The fold enrichment was determined by calculating the Ct values of the MeRIP sample relative to the input sample.

siRNA transfection

A total of 2 × 10^5 cells were seeded into each well of a 6-well plates and grown for 12 h, followed by transfection with the indicated siRNA duplexes, which were delivered using RNAiMAX (Invitrogen) according to the manufacturer's instructions. All the siRNA duplexes were synthesized by RIBOBIO. The single siRNA duplexes were as follows: siNC, siN0000001-1-5 (RIBOBIO); siMETTL3-1, 5′-CAAGTATGTTCACTATGAA-3′; siMETTL3-2, 5′-GACTGCTCTTTCCTTAATA-3′; siYTHDF2-1, 5′-GACCAAGAATGGCATTGCA-3′; siYTHDF2-2, 5′-GCACAGAAGTTGCAAGCAA-3′.

Dual-luciferase reporter assay

The 293T cells were grown in 24-well plates for 24 h, after which the cells were cotransfected with 500 ng of the indicated plasmids, 100 ng of the promoter-reporter plasmid or pGL3-Basic control, and 10 ng Renilla luciferase vector. Firefly and Renilla luciferase activities were analyzed at 24 h post-transfection using the Dual-Luciferase Reporter Assay System (Promega). The relative luciferase activity was calculated as the ratio of firefly luciferase activity to Renilla luciferase activity.

Quantitative reverse-transcription PCR

For gene expression analysis, total cellular RNA was isolated from cultured cells using the TRIzol Reagent and 1 μg of RNA was reverse-transcribed using the GoScript Reverse Transcription System (A5001, Promega) in a 20 μl reaction mixture. The mRNA level was evaluated by real-time PCR using the LightCycler 480 SYBR Green I Master Mix (4887352001, Roche) on a Roche LightCycler 480 instrument. All the gene expression values were normalized to the housekeeping gene ACTB. For the quantification of EBV genome copies, the cellular genomic DNA was isolated from cultured cells using the EZNA DNA kit (D3396-02, Omega BioTek) according to the manufacturer's instructions. EBV copies were detected using qPCR with specific primers targeting the EBV BALF5 gene region, and GAPDH was used as a reference genome copy. The qPCR primers were as follows: KLF4: 5′-ATGCTCGGTCGCATTTTTGG-3′ and 5′-AATTCGCCCGCTCAGATGAA-3′; ACTB: 5′-GTGAAGGTGACAGCAGTCGGT-3′ and 5′-AAGTGGGGTGGCTTTTAGGA-3′; METTL3: 5′-TTGTCTCCAACCTTCCGTAGT-3′ and 5′-CCAGATCAGAGAGGTGGTGTAG-3′; YTHDF2: 5′-GTTGGTAGCGGGTCCATTACT-3′ and 5′-GGTCTTCAGTTTAGGTTGCTGT-3′; BZLF1: 5′-CCCAGTCTCAGACATAACCC-3′ and 5′-CAGGCTGTGGAGCACCAATG-3′; GAPDH-DNA: 5′-GTCAAGGCTGAGAACGGGAA-3′ and 5′-AGCCACACCATCCTAGTTGC-3′; and BALF5-DNA: 5′-CGGAAGCCCTCTGGACTTC-3′ and 5′-CCCTGTTTATCCGATGGAATG-3′.

RNA immunoprecipitation qPCR (RIP-qPCR)

The RIP assay was performed using the Magna RIP Quad RNA-Binding Protein Immunoprecipitation Kit (Millipore, 17-704). For the endogenous METTL3-RIP or YTHDF2-RIP in HK1 and NPEC1-Bmi1 cells, the cells were plated onto a 10 cm dish and grown for 24 h. The cells were then lysed with lysis buffer and 1% of the lysate was left as the input sample. The rest of the lysate was incubated with the anti-METTL3 antibody, anti-YTHDF2 antibody, or a rabbit IgG control conjugated to Protein A/G Dynabeads in 1 ml RIP buffer. After incubation overnight at 4 °C, the beads were washed five times with wash buffer, and the RIP RNA samples and input samples were collected by adding the TRIzol reagent to the beads. The input and all the RIP samples were subjected to qRT-PCR. The relative RIP enrichment was determined by calculating the Ct values of the RIP sample relative to the input sample.

Measurement of total cellular m^{6}A levels

Total RNAs were extracted from the indicated cells using TRIzol reagent. The total m^{6}A content was measured using an m^{6}A RNA methylation quantification kit (cat. no. P-9005; Epigentek) according to the manufacturer instructions. Briefly, 200 ng of each sample and the standard control were bound to the assay wells. The assay wells were incubated with the capture antibody, detection antibody, enhancer solution, detection solution, and stop solution in that order. Finally, the signal was measured using a microplate reader at 450 nm. The relative m^{6}A quantification was calculated according to the standard curve.

Measurement of mRNA stability

The HK1 or NPEC1-Bmi1 cells were transfected with the indicated siRNAs for 24 h. The cells were then treated with actinomycin D (2 μg/ml). RNA was collected at the indicated time after treatment and examined by qRT-PCR. The turnover rates and half-lives of mRNAs were estimated according to previously published methods (71, 72). After actinomycin D treatment, the changes in KLF4 mRNA remaining at the given time relative to 0 h were calculated using the Ct values as described previously. The half-lives were derived from linear regression fitting of ln (relative RNA remaining) as a function of time using the following equation: t1/2 = ln (2)/slope.

Western blot analysis

Western blotting analyses were performed as described previously (67). Briefly, the cells were lysed in RIPA buffer containing a protease inhibitor mixture (Roche) and incubated

on a rocker at 4 °C for 10 min. The protein concentrations of the lysates were measured using a BCA protein assay kit (23227, Pierce) and normalized to equal amounts of protein, separated by SDS-PAGE, transferred to a polyvinylidene difluoride (PVDF) membrane, and incubated with the indicated primary antibodies. Then, PVDF membranes were washed and incubated with species-specific HRP-conjugated secondary antibodies and visualized by enhanced chemiluminescence (ECL, Millipore).

Statistical analysis

The datas were expressed as the means ± SD from at least three independent experiments. Two-group comparisons were conducted using the two-tailed unpaired Student's *t*-test. Statistical analyses were performed using GraphPad Prism 8 (GraphPad Software). In all results, ns denoted "not significant", $^{*}p < 0.05$, $^{**}p < 0.01$ and $^{***}p < 0.001$.

Data availability

The data that support the findings of this study are available from the corresponding author upon reasonable request. The authenticity of this article has been validated by uploading the key raw data onto the Research Data Deposit public platform (www.researchdata.org.cn), under the RDD number RDDB2021001089. The raw sequence data reported in this paper have been deposited in the Genome Sequence Archive of the BIG Data Center at the Beijing Institute of Genomics, Chinese Academy of Science, under accession number HRA000681 (accessible at http://bigd.big.ac.cn/gsa-human).

Supporting information—This article contains supporting information.

Acknowledgments—This study was supported by the National Key R&D Program of China (2017YFA0505600, 2017YFC0908503, and 2016YFA0502100), the National Natural Science Foundation of China (81830090, 81802775, and 82003081), and Guangdong Province Key Research And Development Program (2019B020226002).

Author contributions—T. -L. X. and Z. Z. conceived the original ideas and designed the experiments; D. -L. D., X. L., and L. W. carried out the key experiments; D. -L. D. and T. -L. X. wrote the article with support from L. W. and X. L.; C. X., Y. J., and M. -S. Z. contributed to the sample preparation. All the authors have read and approved the final version of the article.

Conflict of interest—The authors report no conflicts of interest in this work.

Abbreviations—The abbreviations used are: EBV, Epstein–Barr virus; FBS, fetal bovine serum; KLF4, Krüppel-like factor 4; m^{6}A, N6-methyladenosine; NaB, sodium butyrate; METTL3, methyltransferase-like 3; NPC, nasopharyngeal carcinoma; TPA, 12-O-tetradecanoylphorbol-13-acetate.

References

1. Farrell, P. J. (2019) Epstein-Barr virus and cancer. *Annu. Rev. Pathol.* **14**, 29–53
2. Young, L. S., Yap, L. F., and Murray, P. G. (2016) Epstein-Barr virus: More than 50 years old and still providing surprises. *Nat. Rev. Cancer* **16**, 789–802
3. Sun, X. S., Liu, S. L., Liang, Y. J., Chen, Q. Y., Li, X. Y., Tang, L. Q., and Mai, H. Q. (2020) The role of capecitabine as maintenance therapy in de novo metastatic nasopharyngeal carcinoma: A propensity score matching study. *Cancer Commun. (Lond)* **40**, 32–42
4. Wu, C. F., Lv, J. W., Lin, L., Mao, Y. P., Deng, B., Zheng, W. H., Wen, D. W., Chen, Y., Kou, J., Chen, F. P., Yang, X. L., Zheng, Z. Q., Li, Z. X., Xu, S. S., Ma, J., *et al.* (2021) Development and validation of a web-based calculator to predict individualized conditional risk of site-specific recurrence in nasopharyngeal carcinoma: Analysis of 10,058 endemic cases. *Cancer Commun. (Lond)* **41**, 37–50
5. Zhao, Y., Hong, X. H., Li, K., Li, Y. Q., Li, Y. Q., He, S. W., Zhang, P. P., Li, J. Y., Li, Q., Liang, Y. L., Chen, Y., Ma, J., Liu, N., and Chen, Y. P. (2020) ZNF582 hypermethylation promotes metastasis of nasopharyngeal carcinoma by regulating the transcription of adhesion molecules Nectin-3 and NRXN3. *Cancer Commun. (Lond)* **40**, 721–737
6. Henle, W., and Henle, G. (1980) Epidemiologic aspects of Epstein-Barr virus (EBV)-associated diseases. *Ann. N. Y. Acad. Sci.* **354**, 326–331
7. Raab-Traub, N. (2002) Epstein-Barr virus in the pathogenesis of NPC. *Semin. Cancer Biol.* **12**, 431–441
8. Young, L. S. (2020) A novel Epstein-Barr virus subtype associated with nasopharyngeal carcinoma found in South China. *Cancer Commun (Lond)* **40**, 60–62
9. Liu, S. L., Sun, X. S., Li, X. Y., Tang, L. Q., Chen, Q. Y., Lin, H. X., Liang, Y. J., Yan, J. J., Lin, C., Guo, S. S., Liu, L. T., Li, Y., Xie, H. J., Tang, Q. N., Liang, H., *et al.* (2019) The diagnostic and prognostic values of plasma Epstein-Barr virus DNA for residual cervical lymphadenopathy in nasopharyngeal carcinoma patients: A retrospective study. *Cancer Commun. (Lond)* **39**, 14
10. Li, H., Liu, S., Hu, J., Luo, X., Li, N., A, M. B., and Cao, Y. (2016) Epstein-Barr virus lytic reactivation regulation and its pathogenic role in carcinogenesis. *Int. J. Biol. Sci.* **12**, 1309–1318
11. Munz, C. (2019) Latency and lytic replication in Epstein-Barr virus-associated oncogenesis. *Nat. Rev. Microbiol.* **17**, 691–700
12. Bristol, J. A., Djavadian, R., Albright, E. R., Coleman, C. B., Ohashi, M., Hayes, M., Romero-Masters, J. C., Barlow, E. A., Farrell, P. J., Rochford, R., Kalejta, R. F., Johannsen, E. C., and Kenney, S. C. (2018) A cancer-associated Epstein-Barr virus BZLF1 promoter variant enhances lytic infection. *PLoS Pathog.* **14**, e1007179
13. Packham, G., Economou, A., Rooney, C. M., Rowe, D. T., and Farrell, P. J. (1990) Structure and function of the Epstein-Barr virus BZLF1 protein. *J. Virol.* **64**, 2110–2116
14. Schaeffner, M., Mrozek-Gorska, P., Buschle, A., Woellmer, A., Tagawa, T., Cernilogar, F. M., Schotta, G., Krietenstein, N., Lieleg, C., Korber, P., and Hammerschmidt, W. (2019) BZLF1 interacts with chromatin remodelers promoting escape from latent infections with EBV. *Life Sci. Alliance* **2**, e201800108
15. Wille, C. K., Nawandar, D. M., Henning, A. N., Ma, S., Oetting, K. M., Lee, D., Lambert, P., Johannsen, E. C., and Kenney, S. C. (2015) 5-hydroxymethylation of the EBV genome regulates the latent to lytic switch. *Proc. Natl. Acad. Sci. U. S. A.* **112**, E7257–E7265
16. Ramasubramanyan, S., Osborn, K., Al-Mohammad, R., Naranjo Perez-Fernandez, I. B., Zuo, J., Balan, N., Godfrey, A., Patel, H., Peters, G., Rowe, M., Jenner, R. G., and Sinclair, A. J. (2015) Epstein-Barr virus transcription factor Zta acts through distal regulatory elements to directly control cellular gene expression. *Nucleic Acids Res.* **43**, 3563–3577
17. Morrison, T. E., Mauser, A., Wong, A., Ting, J. P., and Kenney, S. C. (2001) Inhibition of IFN-gamma signaling by an Epstein-Barr virus immediate-early protein. *Immunity* **15**, 787–799
18. Rane, M. J., Zhao, Y., and Cai, L. (2019) Krupsilonppel-like factors (KLFs) in renal physiology and disease. *EBioMedicine* **40**, 743–750

19. Luo, W. W., Lian, H., Zhong, B., Shu, H. B., and Li, S. (2016) Kruppel-like factor 4 negatively regulates cellular antiviral immune response. *Cell Mol. Immunol.* **13**, 65–72
20. Yang, L., Liu, X., Song, L., Su, G., Di, A., Bai, C., Wei, Z., and Li, G. (2020) Melatonin restores the pluripotency of long-term-cultured embryonic stem cells through melatonin receptor-dependent m6A RNA regulation. *J. Pineal Res.* **69**, e12669
21. Meyer, K. D., Saletore, Y., Zumbo, P., Elemento, O., Mason, C. E., and Jaffrey, S. R. (2012) Comprehensive analysis of mRNA methylation reveals enrichment in 3' UTRs and near stop codons. *Cell* **149**, 1635–1646
22. Wang, X., Zhao, B. S., Roundtree, I. A., Lu, Z., Han, D., Ma, H., Weng, X., Chen, K., Shi, H., and He, C. (2015) N(6)-methyladenosine modulates messenger RNA translation efficiency. *Cell* **161**, 1388–1399
23. Schwartz, S., Mumbach, M. R., Jovanovic, M., Wang, T., Maciag, K., Bushkin, G. G., Mertins, P., Ter-Ovanesyan, D., Habib, N., Cacchiarelli, D., Sanjana, N. E., Freinkman, E., Pacold, M. E., Satija, R., Mikkelsen, T. S., *et al.* (2014) Perturbation of m6A writers reveals two distinct classes of mRNA methylation at internal and 5' sites. *Cell Rep* **8**, 284–296
24. Dominissini, D., Moshitch-Moshkovitz, S., Schwartz, S., Salmon-Divon, M., Ungar, L., Osenberg, S., Cesarkas, K., Jacob-Hirsch, J., Amariglio, N., Kupiec, M., Sorek, R., and Rechavi, G. (2012) Topology of the human and mouse m6A RNA methylomes revealed by m6A-seq. *Nature* **485**, 201–206
25. Liu, J., Yue, Y., Han, D., Wang, X., Fu, Y., Zhang, L., Jia, G., Yu, M., Lu, Z., Deng, X., Dai, Q., Chen, W., and He, C. (2014) A METTL3-METTL14 complex mediates mammalian nuclear RNA N6-adenosine methylation. *Nat. Chem. Biol.* **10**, 93–95
26. Li, A., Chen, Y. S., Ping, X. L., Yang, X., Xiao, W., Yang, Y., Sun, H. Y., Zhu, Q., Baidya, P., Wang, X., Bhattarai, D. P., Zhao, Y. L., Sun, B. F., and Yang, Y. G. (2017) Cytoplasmic m(6)A reader YTHDF3 promotes mRNA translation. *Cell Res.* **27**, 444–447
27. Wang, X., Lu, Z., Gomez, A., Hon, G. C., Yue, Y., Han, D., Fu, Y., Parisien, M., Dai, Q., Jia, G., Ren, B., Pan, T., and He, C. (2014) N6-methyladenosine-dependent regulation of messenger RNA stability. *Nature* **505**, 117–120
28. Shi, H., Wang, X., Lu, Z., Zhao, B. S., Ma, H., Hsu, P. J., Liu, C., and He, C. (2017) YTHDF3 facilitates translation and decay of N6-methyladenosine-modified RNA. *Cell Res.* **27**, 315–328
29. Courtney, D. G., Kennedy, E. M., Dumm, R. E., Bogerd, H. P., Tsai, K., Heaton, N. S., and Cullen, B. R. (2017) Epitranscriptomic Enhancement of influenza A virus gene expression and replication. *Cell Host Microbe* **22**, 377–386.e375
30. Tirumuru, N., Zhao, B. S., Lu, W., Lu, Z., He, C., and Wu, L. (2016) N(6)-methyladenosine of HIV-1 RNA regulates viral infection and HIV-1 Gag protein expression. *Elife* **5**, e15528
31. Lichinchi, G., Zhao, B. S., Wu, Y., Lu, Z., Qin, Y., He, C., and Rana, T. M. (2016) Dynamics of human and viral RNA methylation during Zika virus infection. *Cell Host Microbe* **20**, 666–673
32. Lichinchi, G., Gao, S., Saletore, Y., Gonzalez, G. M., Bansal, V., Wang, Y., Mason, C. E., and Rana, T. M. (2016) Dynamics of the human and viral m(6)A RNA methylomes during HIV-1 infection of T cells. *Nat. Microbiol.* **1**, 16011
33. Kennedy, E. M., Bogerd, H. P., Kornepati, A. V., Kang, D., Ghoshal, D., Marshall, J. B., Poling, B. C., Tsai, K., Gokhale, N. S., Horner, S. M., and Cullen, B. R. (2016) Posttranscriptional m(6)A editing of HIV-1 mRNAs enhances viral gene expression. *Cell Host Microbe* **19**, 675–685
34. Gokhale, N. S., McIntyre, A. B., McFadden, M. J., Roder, A. E., Kennedy, E. M., Gandara, J. A., Hopcraft, S. E., Quicke, K. M., Vazquez, C., Willer, J., Ilkayeva, O. R., Law, B. A., Holley, C. L., Garcia-Blanco, M. A., Evans, M. J., *et al.* (2016) N6-Methyladenosine in flaviviridae viral RNA genomes regulates infection. *Cell Host Microbe* **20**, 654–665
35. Lu, W., Tirumuru, N., St Gelais, C., Koneru, P. C., Liu, C., Kvaratskhelia, M., He, C., and Wu, L. (2018) N(6)-methyladenosine-binding proteins suppress HIV-1 infectivity and viral production. *J. Biol. Chem.* **293**, 12992–13005
36. Martinez-Perez, M., Aparicio, F., Lopez-Gresa, M. P., Belles, J. M., Sanchez-Navarro, J. A., and Pallas, V. (2017) Arabidopsis m6A demethylase activity modulates viral infection of a plant virus and the m6A abundance in its genomic RNAs. *Proc. Natl. Acad. Sci. U. S. A.* **114**, 10755–10760
37. Hao, H., Hao, S., Chen, H., Chen, Z., Zhang, Y., Wang, J., Wang, H., Zhang, B., Qiu, J., Deng, F., and Guan, W. (2018) N6-methyladenosine modification and METTL3 modulate enterovirus 71 replication. *Nucleic Acids Res.* **47**, 362–374
38. Courtney, D. G., Chalem, A., Bogerd, H. P., Law, B. A., Kennedy, E. M., Holley, C. L., and Cullen, B. R. (2019) Extensive epitranscriptomic methylation of A and C residues on murine leukemia virus transcripts enhances viral gene expression. *mBio* **10**, e01209-19
39. Flemington, E. K., Tsai, K., Courtney, D. G., and Cullen, B. R. (2018) Addition of m6A to SV40 late mRNAs enhances viral structural gene expression and replication. *PLoS Pathog.* **14**, e1006919
40. Tan, B., Liu, H., Zhang, S., da Silva, S. R., Zhang, L., Meng, J., Cui, X., Yuan, H., Sorel, O., Zhang, S. W., Huang, Y., and Gao, S. J. (2018) Viral and cellular N(6)-methyladenosine and N(6),2'-O-dimethyladenosine epitranscriptomes in the KSHV life cycle. *Nat. Microbiol.* **3**, 108–120
41. Ye, F., Chen, E. R., and Nilsen, T. W. (2017) Kaposi's sarcoma-associated herpesvirus utilizes and manipulates RNA N6-adenosine methylation to promote lytic replication. *J. Virol.* **91**, e00466-17
42. Hesser, C. R., Karijolich, J., Dominissini, D., He, C., and Glaunsinger, B. A. (2018) N6-methyladenosine modification and the YTHDF2 reader protein play cell type specific roles in lytic viral gene expression during Kaposi's sarcoma-associated herpesvirus infection. *PLoS Pathog.* **14**, e1006995
43. Imam, H., Khan, M., Gokhale, N. S., McIntyre, A. B. R., Kim, G. W., Jang, J. Y., Kim, S. J., Mason, C. E., Horner, S. M., and Siddiqui, A. (2018) N6-methyladenosine modification of hepatitis B virus RNA differentially regulates the viral life cycle. *Proc. Natl. Acad. Sci. U. S. A.* **115**, 8829–8834
44. Lang, F., Singh, R. K., Pei, Y., Zhang, S., Sun, K., and Robertson, E. S. (2019) EBV epitranscriptome reprogramming by METTL14 is critical for viral-associated tumorigenesis. *PLoS Pathog.* **15**, e1007796
45. Lavi, S., and Shatkin, A. J. (1975) Methylated simian virus 40-specific RNA from nuclei and cytoplasm of infected BSC-1 cells. *Proc. Natl. Acad. Sci. U. S. A.* **72**, 2012–2016
46. Moss, B., Gershowitz, A., Stringer, J. R., Holland, L. E., and Wagner, E. K. (1977) 5'-Terminal and internal methylated nucleosides in herpes simplex virus type 1 mRNA. *J. Virol.* **23**, 234–239
47. Tirumuru, N., and Wu, L. (2019) HIV-1 envelope proteins up-regulate N(6)-methyladenosine levels of cellular RNA independently of viral replication. *J. Biol. Chem.* **294**, 3249–3260
48. Gokhale, N. S., McIntyre, A. B. R., Mattocks, M. D., Holley, C. L., Lazear, H. M., Mason, C. E., and Horner, S. M. (2020) Altered m(6)A modification of specific cellular transcripts affects flaviviridae infection. *Mol. Cell* **77**, 542–555.e8
49. Nawandar, D. M., Wang, A., Makielski, K., Lee, D., Ma, S., Barlow, E., Reusch, J., Jiang, R., Wille, C. K., Greenspan, D., Greenspan, J. S., Mertz, J. E., Hutt-Fletcher, L., Johannsen, E. C., Lambert, P. F., *et al.* (2015) Differentiation-dependent KLF4 expression promotes lytic Epstein-Barr virus infection in epithelial cells. *PLoS Pathog.* **11**, e1005195
50. Shaverdashvili, K., Padlo, J., Weinblatt, D., Jia, Y., Jiang, W., Rao, D., Laczko, D., Whelan, K. A., Lynch, J. P., Muir, A. B., and Katz, J. P. (2019) KLF4 activates NFkappaB signaling and esophageal epithelial inflammation via the Rho-related GTP-binding protein RHOF. *PLoS One* **14**, e0215746
51. Countryman, J. K., Gradoville, L., and Miller, G. (2008) Histone hyperacetylation occurs on promoters of lytic cycle regulatory genes in Epstein-Barr virus-infected cell lines which are refractory to disruption of latency by histone deacetylase inhibitors. *J. Virol.* **82**, 4706–4719
52. Fiches, G. N., Zhou, D., Kong, W., Biswas, A., Ahmed, E. H., Baiocchi, R. A., Zhu, J., and Santoso, N. (2020) Profiling of immune related genes silenced in EBV-positive gastric carcinoma identified novel restriction factors of human gammaherpesviruses. *PLoS Pathog.* **16**, e1008778
53. Luka, J., Kallin, B., and Klein, G. (1979) Induction of the Epstein-Barr virus (EBV) cycle in latently infected cells by n-butyrate. *Virology* **94**, 228–231

54. zur Hausen, H., O'Neill, F. J., Freese, U. K., and Hecker, E. (1978) Persisting oncogenic herpesvirus induced by the tumour promotor TPA. *Nature* **272**, 373–375
55. Morrison, T. E., Mauser, A., Klingelhutz, A., and Kenney, S. C. (2004) Epstein-Barr virus immediate-early protein BZLF1 inhibits tumor necrosis factor alpha-induced signaling and apoptosis by downregulating tumor necrosis factor receptor 1. *J. Virol.* **78**, 544–549
56. Hahn, A. M., Huye, L. E., Ning, S., Webster-Cyriaque, J., and Pagano, J. S. (2005) Interferon regulatory factor 7 is negatively regulated by the Epstein-Barr virus immediate-early gene, BZLF-1. *J. Virol.* **79**, 10040–10052
57. Balan, N., Osborn, K., and Sinclair, A. J. (2016) Repression of CIITA by the Epstein-Barr virus transcription factor Zta is independent of its dimerization and DNA binding. *J. Gen. Virol.* **97**, 725–732
58. Liu, X., Hong, T., Parameswaran, S., Ernst, K., Marazzi, I., Weirauch, M. T., and Fuxman Bass, J. I. (2020) Human virus transcriptional regulators. *Cell* **182**, 24–37
59. Schelcher, C., Valencia, S., Delecluse, H. J., Hicks, M., and Sinclair, A. J. (2005) Mutation of a single amino acid residue in the basic region of the Epstein-Barr virus (EBV) lytic cycle switch protein Zta (BZLF1) prevents reactivation of EBV from latency. *J. Virol.* **79**, 13822–13828
60. Hicks, M. R., Al-Mehairi, S. S., and Sinclair, A. J. (2003) The zipper region of Epstein-Barr virus bZIP transcription factor Zta is necessary but not sufficient to direct DNA binding. *J. Virol.* **77**, 8173–8177
61. Murata, T., Hotta, N., Toyama, S., Nakayama, S., Chiba, S., Isomura, H., Ohshima, T., Kanda, T., and Tsurumi, T. (2010) Transcriptional repression by sumoylation of Epstein-Barr virus BZLF1 protein correlates with association of histone deacetylase. *J. Biol. Chem.* **285**, 23925–23935
62. Winkler, R., Gillis, E., Lasman, L., Safra, M., Geula, S., Soyris, C., Nachshon, A., Tai-Schmiedel, J., Friedman, N., Le-Trilling, V. T. K., Trilling, M., Mandelboim, M., Hanna, J. H., Schwartz, S., and Stern-Ginossar, N. (2019) m(6)A modification controls the innate immune response to infection by targeting type I interferons. *Nat. Immunol.* **20**, 173–182
63. Rubio, R. M., Depledge, D. P., Bianco, C., Thompson, L., and Mohr, I. (2018) RNA m(6) A modification enzymes shape innate responses to DNA by regulating interferon beta. *Genes Dev.* **32**, 1472–1484
64. Xiong, D., Du, Y., Wang, H. B., Zhao, B., Zhang, H., Li, Y., Hu, L. J., Cao, J. Y., Zhong, Q., Liu, W. L., Li, M. Z., Zhu, X. F., Tsao, S. W., Hutt-Fletcher, L. M., Song, E., *et al.* (2015) Nonmuscle myosin heavy chain IIA mediates Epstein-Barr virus infection of nasopharyngeal epithelial cells. *Proc. Natl. Acad. Sci. U. S. A.* **112**, 11036–11041
65. Song, L. B., Zeng, M. S., Liao, W. T., Zhang, L., Mo, H. Y., Liu, W. L., Shao, J. Y., Wu, Q. L., Li, M. Z., Xia, Y. F., Fu, L. W., Huang, W. L., Dimri, G. P., Band, V., and Zeng, Y. X. (2006) Bmi-1 is a novel molecular marker of nasopharyngeal carcinoma progression and immortalizes primary human nasopharyngeal epithelial cells. *Cancer Res.* **66**, 6225–6232
66. Yan, M., Zhang, Y., He, B., Xiang, J., Wang, Z. F., Zheng, F. M., Xu, J., Chen, M. Y., Zhu, Y. L., Wen, H. J., Wan, X. B., Yue, C. F., Yang, N., Zhang, W., Zhang, J. L., *et al.* (2014) IKKalpha restoration via EZH2 suppression induces nasopharyngeal carcinoma differentiation. *Nat. Commun.* **5**, 3661
67. Zhang, H., Li, Y., Wang, H. B., Zhang, A., Chen, M. L., Fang, Z. X., Dong, X. D., Li, S. B., Du, Y., Xiong, D., He, J. Y., Li, M. Z., Liu, Y. M., Zhou, A. J., Zhong, Q., *et al.* (2018) Ephrin receptor A2 is an epithelial cell receptor for Epstein-Barr virus entry. *Nat. Microbiol.* **3**, 1–8
68. Zhang, Y., Liu, T., Meyer, C. A., Eeckhoute, J., Johnson, D. S., Bernstein, B. E., Nusbaum, C., Myers, R. M., Brown, M., Li, W., and Liu, X. S. (2008) Model-based analysis of ChIP-seq (MACS). *Genome Biol.* **9**, R137
69. Dobin, A., Davis, C. A., Schlesinger, F., Drenkow, J., Zaleski, C., Jha, S., Batut, P., Chaisson, M., and Gingeras, T. R. (2013) STAR: Ultrafast universal RNA-seq aligner. *Bioinformatics* **29**, 15–21
70. Li, B., and Dewey, C. N. (2011) RSEM: Accurate transcript quantification from RNA-seq data with or without a reference genome. *BMC bioinformatics* **12**, 323
71. Chen, C. Y., Ezzeddine, N., and Shyu, A. B. (2008) Messenger RNA half-life measurements in mammalian cells. *Methods Enzymol.* **448**, 335–357
72. Huang, H., Weng, H., Sun, W., Qin, X., Shi, H., Wu, H., Zhao, B. S., Mesquita, A., Liu, C., Yuan, C. L., Hu, Y. C., Huttelmaier, S., Skibbe, J. R., Su, R., Deng, X., *et al.* (2018) Recognition of RNA N(6)-methyladenosine by IGF2BP proteins enhances mRNA stability and translation. *Nat. Cell Biol.* **20**, 285–295

ASBMB